

Phonon dispersion at the Be(0001) surface

J. B. Hannon* and E. J. Mele

Department of Physics, University of Pennsylvania, Philadelphia, Pennsylvania 19104-6396

E. W. Plummer

Department of Physics and Astronomy, University of Tennessee, Knoxville, Tennessee 37996-1200

and Oak Ridge National Laboratory, P.O. Box 2008, Oak Ridge, Tennessee 37831-6057

(Received 18 May 1995)

Measurements of surface-phonon dispersion at the Be(0001) surface are reported that are found to differ significantly from the predictions of an accurate model of the truncated bulk: the sign of the Rayleigh wave dispersion along the zone boundary is reversed in theory and experiment. The measured dispersion implies a reduction in the magnitude of noncentral forces at the surface. Such a reduction is compatible with the electronic structure of the Be(0001) surface, which is more free-electron-like than that of bulk Be due to a high density of surface states. We conclude that the properties of the surface states dominate the dynamics of surface atoms.

I. INTRODUCTION

Be is an interesting material, because many of the physical properties are anomalous compared to those of other elements. The properties of bulk Be are a result of the unique position of Be in the Periodic Table: second row and second column. This gives rise to unusual bonding characteristics, which can be illustrated by comparing the properties of He, Be, and Mg. The valence shells of these elements are s like and closed ($2s^2$ for Be). In the simplest conceptual picture, as two atoms are brought together to form a dimer the bonding and antibonding states formed from the overlap of the closed s shells are both fully occupied, and dimer ground state is formally repulsive. As expected, the binding energy of alkaline-earth-metal dimers is small: 0.1 eV for Be_2 (Ref. 1) and 0.05 eV for Mg_2 (Ref. 2). The ability of second-column elements to form bonds depends on the ability to “promote” an electron from the closed s shell to an unoccupied p or d level. The cost of promotion is offset by the energy-gain associated with s - p (or s - d) hybridization. This hybridization is highly sensitive to the local atomic geometry: the energy per bond in bulk Be (12 near neighbors) is nearly three times larger than the binding energy of the Be dimer. For He, the energy cost of promotion is so large that metallic bonding is not possible. However, for both Be and Mg, the promotion energy is comparatively small (Mg: 2.6; Be: 2.8 eV), and stable hcp phases exist at room temperature. Despite the fact that the s -to- p promotion energies of Be and Mg are nearly equal, the cohesive energy of bulk Be is nearly 3 times larger than that of Mg.³ The increased bond strength of Be reflects the dramatic energy lowering of the unoccupied p states in the highly coordinated bulk environment. Be is a second-row element, and as such, has an entirely s -like core ($1s^2$), which presents no orthogonalization barrier to states derived from atomic p levels. This leads to enhanced hybridization of s and p states relative to that occurring for Mg. This can be most easily illustrated by comparing the calculated electronic density of states (DOS). The DOS for bulk Be is nearly free-electron-like, whereas that of bulk Be

is nearly semiconducting, with a minimum in the DOS near the Fermi level (Fig. 1). Furthermore, the c/a ratio, which characterizes the hcp crystal structure, is 4% smaller for Be than for Mg. The c/a ratio of Mg is equal to the “ideal” value (calculated from the packing of hard spheres), and consequently the nearest in- and out-of-plane neighbors are equidistant. However, in Be, the bonds to out-of-plane neighbors are shorter. Chou, Lam, and Cohen have shown that the small c/a ratio of Be is associated with an anisotropy in the p -derived DOS.⁴

The bonding between atoms in a solid determines the dis-

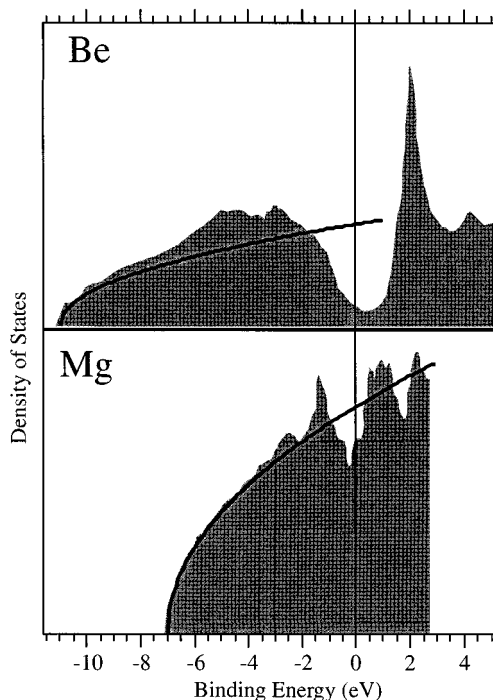


FIG. 1. Calculated electronic density of states for bulk Be (Ref. 4) and Mg (Ref. 3). Solid lines indicate the corresponding free-electron densities of state.

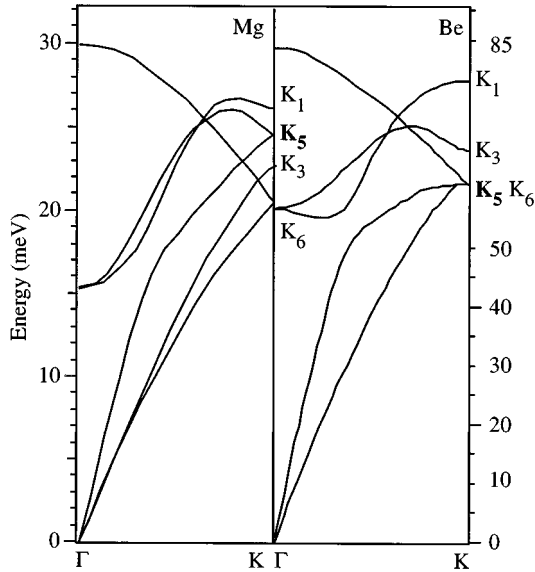


FIG. 2. The measured bulk phonon dispersion along the Γ - K direction for Mg (Ref. 12) and Be (Ref. 13).

persion of vibrational modes. For bulk Be, the directional nature of the bonding leads to phonon dispersion, which is very different from that of other hcp metals. The differences arise because the electronic DOS of bulk Be is more like that of a covalently bonded semiconductor: the density of states is low at the Fermi energy, and the Fermi surface is nonspherical.⁵ The vibrational motion of the ions leads to restoring forces arising from both the direct ion-ion interaction, as well as the screening response of the valence electron distribution. When the electronic screening of the ion motion is anisotropic, noncentral forces result. This is common for semiconductors, where noncentral interactions are often modeled using phenomenological “angle-bending” forces,^{6,7} or as interactions between ions and interstitial “bond charges,”^{8,9} or higher-order electrostatic multipoles.¹⁰

For hcp materials, the influence of noncentral forces can be inferred directly from the bulk phonon dispersion.¹¹ In Fig. 2, the dispersion of bulk phonons modes for Be (Ref. 13) and Mg (Ref. 12) is shown for momentum parallel to the line Γ to K in the bulk Brillouin zone. The symmetry of the K point in the bulk zone is such that the energies of the six bulk phonon modes are functions of only four independent interaction constants.¹⁴ Four of the modes involve circular motion (K_1, K_3, K_5) of the ions parallel to the (0001) planes, and the remaining two are polarized perpendicular to the (0001) planes (K_6). Roy *et al.* have shown that for any model based on pairwise central interactions, one of the four parameters is identically zero.¹¹ This restriction leads to an ordering of the circularly polarized modes, which is characteristic of all central-force (CF) models: the energy of the doubly degenerate K_5 mode always falls in between those of the K_1 and K_3 modes, as is seen for Mg. The measured bulk phonon dispersion of Be does not exhibit the CF ordering,¹³ and consequently, any quantitative description of the lattice dynamics requires a model that incorporates noncentral interactions. Our modeling shows that, for Be, the anomalous ordering of modes at the K point is largely determined by the

interaction between nearest neighbors within the (0001) planes, that is, by the noncentral nature of in-plane forces.

The strong dependence of s - p hybridization on coordination and local geometry raises interesting questions about the bonding in Be structures of reduced dimensionality. First-principles calculations for the Be dimer, hexagonal monolayer, and hcp dilayer indicate a strong dependence of the electronic and structural properties on the local geometry.^{1,15,16} For example, the calculated cohesive energy of the Be monolayer is nearly that of bulk Be (2.94 eV vs 3.34 eV for bulk Be),¹⁵ whereas the bonding between planes in the Be dilayer is weaker than that of bulk Be.¹⁶ At a crystal surface, one can experimentally probe cohesion in such a low-dimensional structure. We have studied the structure and dynamics at Be surfaces in order to better understand the effects of reduced coordination on the bonding of Be atoms. In this paper, we report on measurements of the phonon dispersion at the close-packed (0001) surface. Our investigation was motivated by the analysis of low-energy electron diffraction (LEED) data, which indicates that the surface layer is expanded outward by nearly 6%.¹⁷ Large relaxations at close-packed surfaces are unusual, and based on charge-smoothing arguments, one expects only a small (inward) relaxation at the surface.¹⁸ The measurement of surface-phonon dispersion can provide more detailed information on the bonding at the surface, because the energy cost associated with the symmetric distortions of the lattice are closely related to the bonding and stability of the surface. We find that the vibrations at the Be(0001) surface are qualitatively different from the predictions of an accurate bulk-terminated (BT) model. Most significantly, the sign of the measured Rayleigh wave (RW) dispersion along the zone boundary is not correctly reproduced in the BT calculation. The correct RW dispersion is only obtained if noncentral forces are substantially reduced in magnitude at the surface. This runs counter to the expectation that noncentral forces are enhanced at the surface: Eguiluz and co-workers have shown that the abrupt termination of the charge density normal to a metal surface leads to inherently anisotropic screening, and to enhanced noncentral forces.^{19,20} However, for the Be(0001) surface, a reduction in the in-plane noncentral forces at the surface is consistent with our knowledge of the surface electronic structure, which is dominated by the existence of a large number of surface states. As is illustrated in Fig. 3, surface states increase the DOS at the Fermi energy (E_F) by nearly a factor of 5 in the surface layer,²¹ and consequently screening in the surface region is more efficient than in bulk Be. In addition, the surface-induced DOS is more isotropic than that of bulk Be. In short, the Be(0001) surface is a high-density, free-electron metal ($r_s=1.9$), whereas bulk Be is nearly semiconducting.

II. EXPERIMENT

The data presented in this paper were obtained from two mechanically polished samples cut from separate Be boules. One of these crystals was also used for a structural study of the Be(0001) surface.¹⁷ Surface-phonon dispersion measurements were performed using a standard ultrahigh vacuum chamber equipped with an electron-energy-loss spectrometer capable of energy resolution below 2.0 meV. A clean, well-

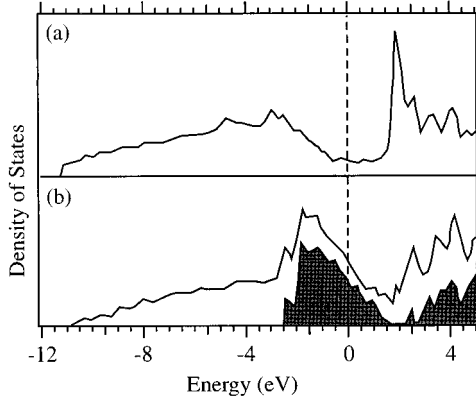


FIG. 3. Calculated layer-resolved DOS for the (a) central layer and (b) surface layer of a nine-layer Be(0001) slab (Ref. 21). Shaded region indicates the contribution from surface states.

ordered Be(0001) surface was prepared via repeated cycles of 1.0 keV Ne ion bombardment at a temperature of 450 °C, followed by annealing periods also at 450 °C. Adsorption of contaminants was monitored using electron-energy-loss spectroscopy (EELS) and auger-electron spectroscopy. LEED was used to align the EELS scattering plane to the high-symmetry directions of the (0001) surface.

We have measured EELS spectra along the high-symmetry directions of the Be(0001) surface for a number of impact energies in the range 20–150 eV. This was done so as to exclude primary energies for which bulk modes might have anomalously large cross sections. Most of the data presented in this paper were recorded using impact energies in the range 40 to 80 eV for which the RW cross section near the zone boundary was largest.

An EELS spectrum sampling the \bar{K} point in the surface Brillouin zone is shown in Fig. 4. The solid line, determined by a fit to the measured feature, is a Lorentzian line shape (FWHM = 1.4 meV) convolved with the elastic peak. A series of EELS spectra for parallel momenta along the line

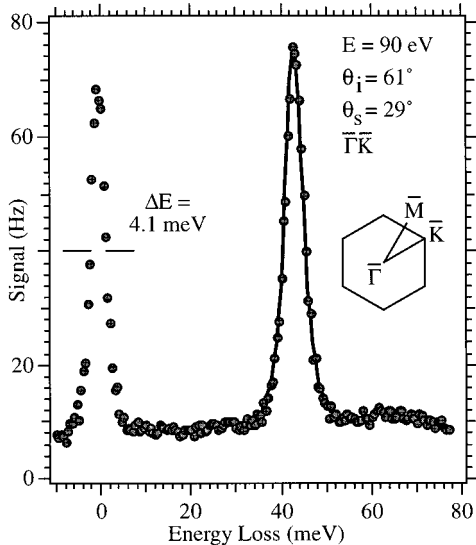


FIG. 4. EELS spectrum sampling a point near \bar{K} . The solid line is a Lorentzian line shape convolved with the elastic peak. The inset shows the Be(0001) surface Brillouin zone.

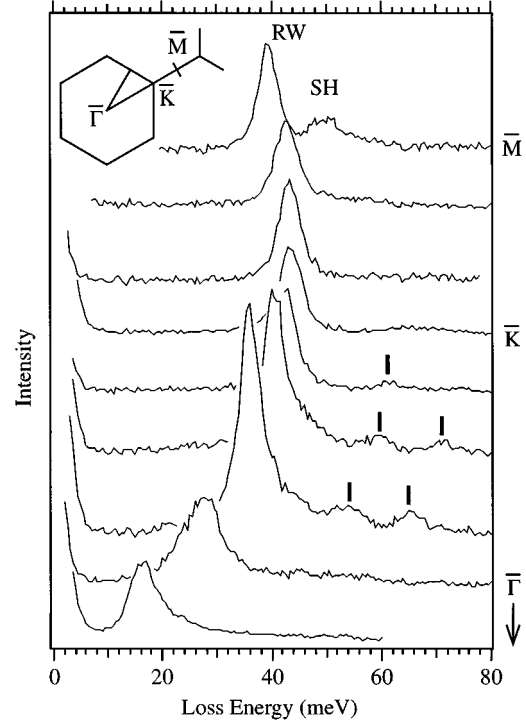


FIG. 5. EELS spectra illustrating surface-mode dispersion along the line $\bar{\Gamma}-\bar{K}-\bar{M}$. Weaker surface modes are indicated by vertical lines. The Rayleigh wave (RW) and shear-horizontal mode (SH) are indicated.

$\bar{\Gamma}-\bar{K}-\bar{M}$ are shown in Fig. 5. For these spectra the scattering plane was aligned along the $\bar{\Gamma}-\bar{K}$ direction, that is, along the line joining in-plane nearest neighbors. The intense dispersing feature is the RW, which in the long-wavelength limit ($q \rightarrow 0$) corresponds to the surface acoustic mode that can be calculated using continuum elastic theory. Along the edges of the zone ($\bar{K}-\bar{M}$), the RW consists of motion of the top-layer atoms normal to the surface. At the \bar{M} point, a second mode is observed at roughly 50 meV. This mode is a shear-horizontal (SH) vibration, which is polarized entirely within the (0001) plane. Several weaker, high-energy modes are also observed. These modes reside near the edges of gaps in the continuum of surface-projected bulk bands and are surface resonances.

III. LATTICE DYNAMICS OF BULK Be AND Be(0001)

We have modeled the lattice dynamics of bulk Be and Be(0001) using a Born–von Karman scheme, in which the potential energy of the lattice is expanded to second order in the ion displacements, u_i^α :

$$E = \frac{1}{2} \sum_{\substack{i,j \\ \alpha,\beta}} \Phi_{\alpha\beta}(i,j) u_i^\alpha u_j^\beta,$$

where

$$\Phi_{\alpha\beta}(i,j) = \frac{\partial^2 E}{\partial u_i^\alpha \partial u_j^\beta}.$$

TABLE I. Force constants for the noncentral force model of bulk Be, in N/m, determined from a fit to the neutron scattering data of Stedman *et al.* (Ref. 13). The matrices shown correspond to atoms that are linked by the unit vectors found in the left-hand column. The z axis of the slab is parallel to the c axis of the hcp crystal structure.

Neighbor number $\hat{r}_{n,m}=(x,y,z)$	$\Phi(n,m)=\begin{bmatrix} n_x m_x & n_x m_y & n_x m_z \\ n_y m_x & n_y m_y & n_y m_z \\ n_z m_x & n_z m_y & n_z m_z \end{bmatrix}$ N/m		
1NN +0.59, +0.00, -0.81	$\begin{bmatrix} \alpha_1 & \delta_1 \\ & \beta_1 \\ \delta_1 & \gamma_1 \end{bmatrix}$	$\alpha_1 = -11.93$ $\gamma_1 = -19.59$	$\beta_1 = -3.98$ $\delta_1 = +13.33$
2NN +0.00, +1.00, +0.00	$\begin{bmatrix} \alpha_2 & \delta_2 \\ -\delta_2 & \beta_2 \\ & \gamma_2 \end{bmatrix}$	$\alpha_2 = -3.15$ $\gamma_2 = -1.29$	$\beta_2 = -19.14$ $\delta_2 = -6.92$
3NN -0.83, +0.00, +0.56	$\begin{bmatrix} \alpha_3 & \delta_3 \\ & \beta_3 \\ \delta_3 & \gamma_3 \end{bmatrix}$	$\alpha_3 = -1.56$ $\gamma_3 = +0.13$	$\beta_3 = +2.35$ $\delta_3 = +4.45$
4NN +0.00, +0.00, -1.00	$\begin{bmatrix} \alpha_4 & \\ & \alpha_4 \\ & & \beta_4 \end{bmatrix}$	$\alpha_4 = -2.20$	$\beta_4 = -4.67$
5NN -0.67, +0.58, +0.46	$\begin{bmatrix} \alpha_5 & \epsilon_5 & \delta_5 \\ \epsilon_5 & \beta_5 & \lambda_5 \\ \delta_5 & \lambda_5 & \gamma_5 \end{bmatrix}$	$\alpha_5 = -1.48$ $\gamma_5 = -0.327$ $\epsilon_5 = +0.46$	$\beta_5 = -0.55$ $\delta_5 = +2.15$ $\lambda_5 = -0.14$
6NN +1.00, +0.00, +0.00	$\begin{bmatrix} \alpha_6 & \\ & \beta_6 \\ & & \gamma_6 \end{bmatrix}$	$\alpha_6 = -1.76$ $\gamma_6 = -0.75$	$\beta_6 = +1.34$
7NN +0.00, +0.54, +0.84	$\begin{bmatrix} \alpha_7 & -\epsilon_7 & -\delta_7 \\ \epsilon_7 & \beta_7 & \lambda_7 \\ \delta_7 & \lambda_7 & \gamma_7 \end{bmatrix}$	$\alpha_7 = +0.19$ $\gamma_7 = +0.33$ $\epsilon_7 = -0.77$	$\beta_7 = -0.09$ $\delta_7 = +1.12$ $\lambda_7 = -0.50$

The indices α and β label the Cartesian coordinates, and i and j specify the ions. The fundamental quantities of the model are the 3×3 matrices $\Phi_{\alpha\beta}(i,j)$, which describe the interaction between atoms i and j . Typically, a particular form for the interaction between two ions is assumed [i.e., a central force: $E=V(r)$] and the matrices Φ are calculated analytically. However, one can also determine the matrices from a fit to the measured dispersion. The advantage of this approach is that one is guaranteed to reproduce the measured dispersion provided the range of interaction is chosen to be large enough. The form of the matrices Φ are restricted by the symmetry of the lattice, and one can determine the independent parameters from symmetry considerations.^{22,23} For bulk Be, the forms of the matrices for the first- through seventh-nearest neighbors (1NN–7NN) are given in Table I, along with the values of the parameters determined by a fit to the neutron scattering data of Stedman *et al.*¹³ The calculated

and measured bulk phonon dispersion along the high-symmetry directions of the bulk zone are shown in Fig. 6.

We have investigated the uniqueness of the fit by varying the range of interaction as well as the initial values of the parameters. From the parameter values given in Table I, it is evident that the forces are “large” for the first three or four neighbor shells, beyond which the interactions are much weaker. Consequently, the minimum model that can qualitatively describe the bulk lattice dynamics requires interactions out to fourth-nearest neighbor.²⁴ If more neighbor shells are included, quantitative agreement between the model and the measured dispersion improves. However, the values of the parameters for the near-neighbor interactions do not change significantly. Beyond tenth-nearest neighbor, the large number of free parameters begins to destabilize the fitting process. We have included a relatively large number of neighbor shells in order to arrive at a quantitatively correct description of the bulk lattice dynamics.

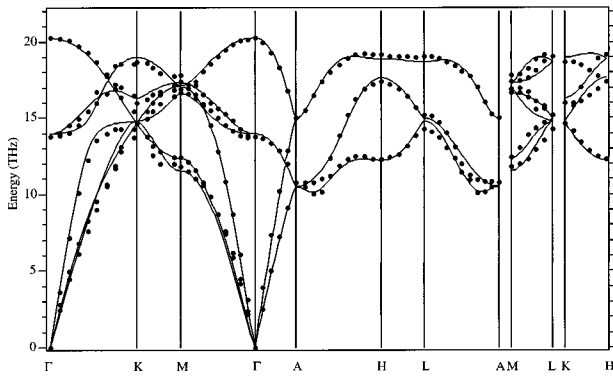


FIG. 6. Bulk phonon dispersion along the high-symmetry directions of the hcp Brillouin zone. The measured dispersion (Ref. 13) (filled circles) is compared to that calculated using the noncentral model with parameters given in Table I.

For a model based exclusively on central interactions, each force-constant matrix is a function of, at most, two parameters. In addition, some of the model parameters are identically zero for any CF model. This is the case for the δ_2 parameter of the 2NN interaction. From our fit to the bulk lattice dynamics, we find that a large, nonzero value of δ_2 is required in order to arrive at the correct ordering of bulk modes at K . Physically, δ_2 describes the coupling between the perpendicular displacements of in-plane nearest neighbors (Fig. 7). In a CF model, when atom A is displaced parallel to an in-plane bond, the symmetry of the interaction potential results in a force on atom B which is always directed along the bond [Fig. 7(a)]. However, if the response of the valence electron distribution is anisotropic, then the charge density induced by the displacement of atom A can lead to a resultant force on atom B with components both perpendicular and parallel to the bond [Fig. 7(b)]. It is primarily this coupling that leads to the observed ordering of modes at K in bulk Be. At the Be(0001) surface, where the surface states make the charge density more isotropic, we find that the measured surface-phonon dispersion is consistent with a purely central interaction: $\delta_2=0$.

IV. VIBRATIONAL MODES AT THE Be(0001) SURFACE

The measured phonon dispersion along the high-symmetry directions of the Be(0001) surface is shown in Fig.

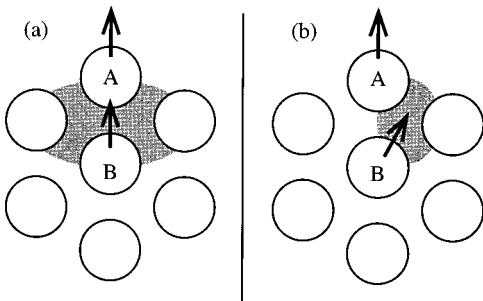


FIG. 7. Arrows indicate the force on atom B when atom A is displaced assuming (a) central-force interactions, and (b) non-central interactions. Shaded area indicates schematically the charge density induced by the displacement of atom A .

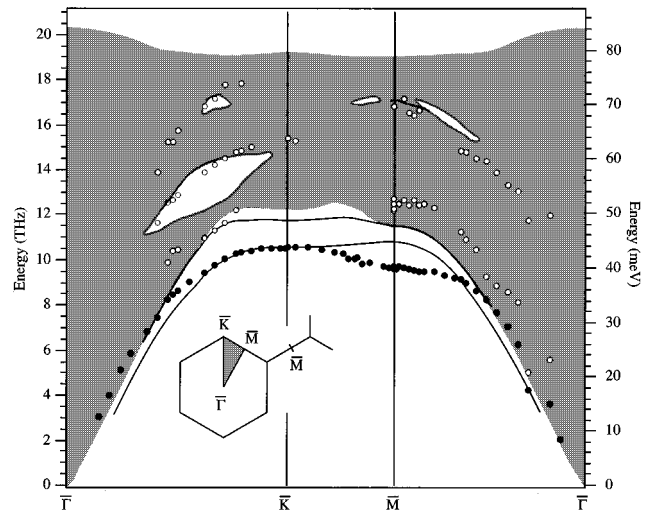


FIG. 8. Dispersion of vibrational modes at the Be(0001) surface. The filled (open) circles indicate intense (weak) features in the measured dispersion. Solid lines indicate the calculated dispersion of surface modes for a bulk-terminated 500-layer slab. The shaded area corresponds to the projection of bulk phonon modes onto the (0001) surface.

8, superimposed on the calculated vibrational modes for a 500-layer Be slab. The calculated surface modes are in qualitative agreement with the unpublished Green's function calculation of Sameth and Mele.^{25,26} In that calculation, a pairwise harmonic model, which is constrained to agree with measured bulk dispersion at the high-symmetry points in the Brillouin zone, is applied to the semi-infinite surface. We take the agreement between our calculation and that of Sameth and Mele as evidence that the application of our bulk model to the slab geometry has been implemented correctly. The shaded regions of Fig. 8 represent the projection of bulk phonon modes onto the (0001) surface, and the solid lines indicate the calculated dispersion of surface-localized vibrational modes and resonances. Surface modes are defined as those modes for which the displacements in the top two layers comprise more than 50% of the total displacement. Since the model parameters have not been modified in the surface region, the calculated phonon dispersion shown in Fig. 8 corresponds to a BT surface.

Two surface modes, split off below the bulk-band edge, are present in the BT calculation. The lowest-lying surface mode is the RW, and the upper mode, just at the band edge, has displacements parallel to the surface. The RW consists mainly of motion normal to the surface, with a penetration depth that increases with increasing wavelength; near the $\bar{\Gamma}$ point, the RW penetrates far into the bulk, whereas along the zone boundary ($\bar{K}-\bar{M}$), it is highly surface localized. At \bar{M} , the parallel mode is a shear-horizontal vibration. At \bar{K} , the motion is circularly polarized. A discussion of the agreement between theory and experiment for these modes is deferred to the following sections.

There are several higher-lying surface modes that are situated close to, or within, gaps in the projected bulk-band density. In order to reproduce these modes in a calculation, one requires a model that correctly reproduces the band gaps. Because these modes are situated near the projected bulk

TABLE II. Calculated surface-mode eigenvectors at \bar{M} and \bar{K} for the bulk-terminated Be(0001) surface. The displacement amplitudes (A) are normalized to unity, and the phases (ϕ) are given in degrees. The longitudinal mode at \bar{M} is representative of a high density of surface-localized modes at this energy.

	\bar{M}						\bar{K}			
	Rayleigh 44.6 meV		Shear 47.5 meV		Longitudinal 70.9 meV		Rayleigh 43.7 meV		Parallel 48.5 meV	
	A	ϕ	A	ϕ	A	ϕ	A	ϕ	A	ϕ
x_1	0.07	+0	0.00	+0	0.10	+120	0.00	+0	0.57	+0
y_1	0.00	+0	0.59	+0	0.00	+0	0.00	+0	0.57	+90
z_1	0.91	+0	0.00	+0	0.06	+120	0.92	+0	0.00	+0
x_2	0.13	+60	0.00	+0	0.20	+0	0.27	+180	0.00	+0
y_2	0.00	+0	0.45	+60	0.00	+0	0.27	+90	0.00	+0
z_2	0.33	+60	0.00	+0	0.12	+0	0.00	+0	0.47	+180
x_3	0.00	+0	0.00	+0	0.05	+120	0.00	+0	0.24	+180
y_3	0.00	+0	0.37	+0	0.00	+0	0.00	+0	0.24	-90
z_3	0.15	+0	0.00	+0	0.07	+120	0.06	+90	0.00	+0
x_4	0.01	+0	0.00	+0	0.10	+0	0.03	+180	0.00	+0
y_4	0.00	+0	0.31	+60	0.00	+0	0.03	+90	0.00	+0
z_4	0.09	+60	0.00	+0	0.09	+0	0.00	+0	0.12	+0
x_5	0.00	+0	0.00	+0	0.03	-60	0.00	+0	0.07	+0
y_5	0.00	+0	0.26	+0	0.00	+0	0.00	+0	0.07	+90
z_5	0.04	+0	0.00	+0	0.08	+120	0.01	+0	0.00	+0

density, they have relatively large penetration depths. That is, the higher-lying surface modes are more sensitive to the bulk environment than the low-lying RW. To illustrate this point, the displacement patterns of the surface modes at \bar{K} and \bar{M} are given in Table II.²⁷ The high-energy mode at \bar{M} is a longitudinal resonance that penetrates well beyond the fourth layer of the crystal.

A. The long-wavelength Rayleigh wave dispersion

As the wavelength of the RW is increased, the displacement pattern extends farther into the bulk. In the long-wavelength limit, the energy of the RW is a linear function of the momentum transfer, with a slope which can be expressed in terms of the bulk elastic properties. This is the case, because the RW mode is a superposition of transverse and longitudinal bulk waves, which satisfy the surface boundary conditions. However, we find that the slope of the measured RW dispersion is roughly 35% larger than that of the calculated RW dispersion (Fig. 9). Since the RW mode falls entirely within the projected bulk band density, one must be sure that the feature that is measured corresponds to the RW, and not to a high density of bulk modes. Since the width of the loss feature increases significantly when the bulk density is penetrated (Fig. 10), coupling to bulk modes may be important. These issues can be addressed by comparing the measured EELS spectra to the calculated density of vibrational states at the surface. This latter quantity is computed by weighting each mode of a 500-layer slab by the amplitude of vibration (in a given direction) in the surface region, defined here as the top two layers of the slab. In Fig. 11, an EELS spectra corresponding to a momentum transfer of $0.17\bar{M}$ is shown with the corresponding surface-weighted density of states computed for displacements along the following directions: normal to the surface (“normal”), perpen-

dicular to both the wave vector and the surface normal (“shear”), and parallel to the wave vector (“longitudinal”). The largest feature in the normal-weighted DOS is the RW, situated just below the bulk-band edge at 9.5 meV. The measured feature, at 14 meV, is significantly higher in energy than the calculated RW. Since the density of bulk modes in the vicinity of the RW is small, it is unlikely that the measured loss feature is a superposition of more than one mode.

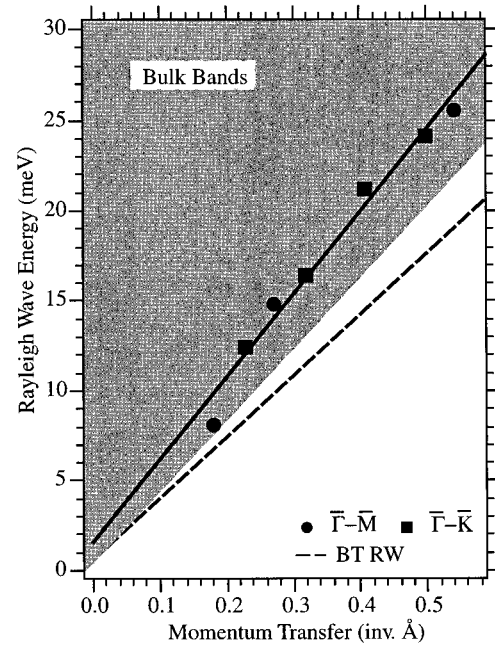


FIG. 9. Comparison of the calculated (dashed line) and measured (solid line) long-wavelength RW dispersion along the high-symmetry directions of the Be(0001) surface. Circles (squares) indicate measurements from the $\bar{\Gamma}\bar{M}$ ($\bar{\Gamma}\bar{K}$) direction.

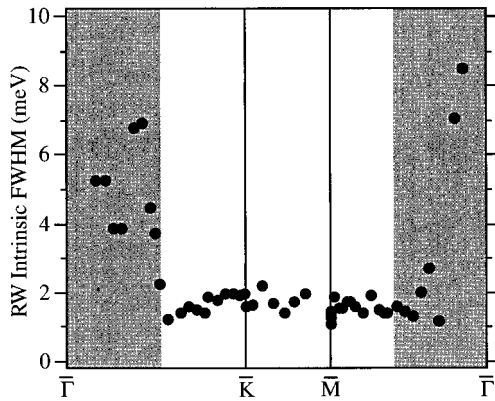


FIG. 10. Filled circles indicate the FWHM of the RW loss, after deconvolution of the instrumental resolution, along the high-symmetry directions of the (0001) surface. Shaded area corresponds to wave vectors for which the RW feature is situated within the projected bulk-band density.

The largest feature in the shear density, at 12 meV, is the shear-horizontal surface mode, which should not be excited using this scattering geometry, because it is odd under reflection in the scattering plane. One can also see that the feature measured at 21 meV corresponds to a high density of longitudinal modes. The calculated DOS shows that the contribution of bulk modes to the measured loss feature at 14 meV cannot account for the discrepancy between the calculated and measured losses. A similar conclusion holds for the long-wavelength RW dispersion along the $\bar{\Gamma}-\bar{K}$ direction; there is an intrinsic “stiffening” of the long-wavelength RW dispersion compared to that calculated using the BT theory.

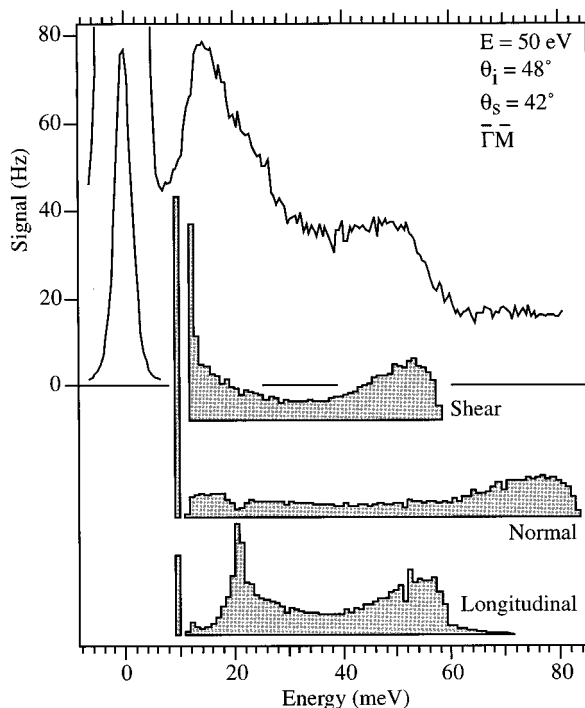


FIG. 11. EELS spectrum for momentum transfer of 0.27 \AA^{-1} along the $\bar{\Gamma}\bar{M}$ direction ($0.17\bar{\Gamma}\bar{M}$) compared to the surface-weighted DOS from the bulk-terminated calculation.

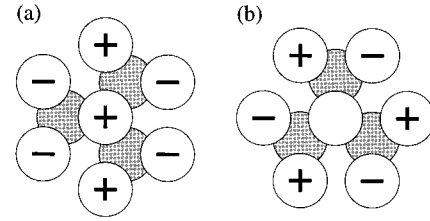


FIG. 12. Rayleigh wave displacement patterns at (a) \bar{M} and (b) \bar{K} . The planes of constant phase move from left to right across the page.

From the point of view of continuum elastic theory, a stiffening of the RW dispersion can have two origins. One possibility is that the influence of the surface extends beyond the first or second surface layer, essentially modifying the “bulk” elastic properties that enter the RW dispersion. Measurement of surface core-level shifts indicate that this is indeed the case: three shifted surface core levels have been measured²⁸ and calculated²⁹ at the Be(0001) surface, indicating that the chemical environment of the first few surface layers is not “bulklike.” In comparison, the surface core levels of the Al(111) surface exhibit no measurable shift in binding energy.³⁰ A second possible mechanism behind the large slope of the RW dispersion is surface stress. The boundary conditions at the solid-vacuum interface are modified when the surface is subject to either tensile or compressive stress.³¹ Stress may be particularly important for the Be(0001) surface; first-principles calculations indicate that tensile stress at the Be(0001) is extremely large.²⁹ No attempt has been made to adjust the parameters of our microscopic model in order to reproduce the observed long-wavelength dispersion for two reasons: the parameter space of possible modifications is large, and the effects of surface stress cannot be taken into account unambiguously using our model. The discrepancy between the measured and calculated RW dispersion at long wavelengths could perhaps be resolved if the model parameters were calculated from first principles.

B. Rayleigh wave dispersion at the zone boundary

The most striking discrepancy between the BT theory and the measurements concerns the dispersion of the RW along the zone boundary ($\bar{K}-\bar{M}$). The measured RW energy at \bar{M} is lower than that at \bar{K} , whereas the opposite is found in the BT calculation. This discrepancy is unusual in the sense that it is directional: the RW energy is too low at \bar{M} , but not at \bar{K} . In fact, as one proceeds around the edge of the hexagonal zone, the measurements and the BT calculation are completely out of phase. What is commonly observed when measured RW dispersion is compared to BT theory is that the RW dispersion is too high throughout the entire Brillouin zone.³² One can then invoke weaker or stronger interplanar bonding (or surface stress), i.e., modify a central interaction, in order to reproduce the observed dispersion. At both \bar{K} and \bar{M} the RW consists almost entirely of motion of the top layer normal to the surface (Fig. 12). Since the displacement patterns are similar, i.e., the same bonds are stretched in the motion, modifications to the central interactions are likely to effect both modes in the same way. It is unlikely that the

effect of modifying a central interaction is to increase the energy of the RW at \bar{M} , while having no effect on the RW at \bar{K} . The dependence of the RW dispersion from \bar{K} to \bar{M} on the details of the central and noncentral parts of the interaction is addressed in detail below.

In order to understand the apparent stiffening of the RW near the \bar{M} point, one must examine the displacement patterns, given numerically in Table II, more closely. The \bar{M} point is contained within a mirror plane of the surface, and consequently all vibrational modes are either odd or even under reflection within the plane. The RW is even under reflection, and the in-plane displacements of all atoms are parallel. However, at \bar{K} , the modes are combinations of perpendicular motion and in-plane circular motion; that is, the in-plane displacements have both parallel and perpendicular components. The differences between the motion at \bar{K} and \bar{M} become more significant when one considers the phonon dispersion of bulk Be. In the Introduction, it was shown that the ordering of bulk modes at K is not consistent with purely central interactions. From our fit to the bulk phonon dispersion, we find that the largest noncentral interaction is that which couples the perpendicular in-plane displacements of in-plane neighbors (Fig. 7). The circularly polarized bulk modes at K are very sensitive to this coupling (δ_2 parameter from Table I), which is large in our model, whereas motion perpendicular to the plane is not. We find that it is precisely this interaction that is responsible for the discrepancy between the calculated and measured RW dispersion from \bar{K} to \bar{M} . The effect of two modifications to the model on the RW dispersion from \bar{K} to \bar{M} are illustrated in Fig. 13. In panel (a), the bulk-terminated dispersion is shown for reference. The effect of fixing $\delta_2=0$ in the top two layers of the slab is shown in panel (b). Only this parameter has been changed; all others are taken from the fit to the bulk dispersion. The RW at \bar{K} moves up significantly in energy, while the RW at \bar{M} shows a small stiffening. The slope of the dispersion from \bar{K} to \bar{M} reverses, and becomes slightly negative. The implication of this change is that the in-plane forces in the surface region are more “central” than those of bulk Be, and, therefore, that the electronic environment is more isotropic within the surface plane. This conclusion runs counter to the expectation that noncentral forces are enhanced at a surface. Eguluz and co-workers have shown that the abrupt decay of the charge density normal the surface leads to anisotropic screening and to larger noncentral interactions.^{19,20} However, for Be(0001), a reduction of the noncentral forces is plausible, given our knowledge of the electronic structure of the Be(0001) surface. The large enhancement to the DOS near the Fermi energy makes the surface DOS more free-electron-like and isotropic within the plane (Fig. 3). Furthermore, the observed RW dispersion from \bar{K} to \bar{M} is similar to that measured at the fcc(111) surfaces of most noble metals, all of which are adequately described using CF models.³² The connection between the RW dispersion and the circularly polarized K_5 mode can be illustrated using a bulk calculation. If one calculates the bulk phonon dispersion with $\delta_2=0$, and the remaining parameters taken from Table I, one finds that the K_5 mode moves up in energy by roughly 6 meV, falling between the K_1 and K_3 modes. The modes at M are not

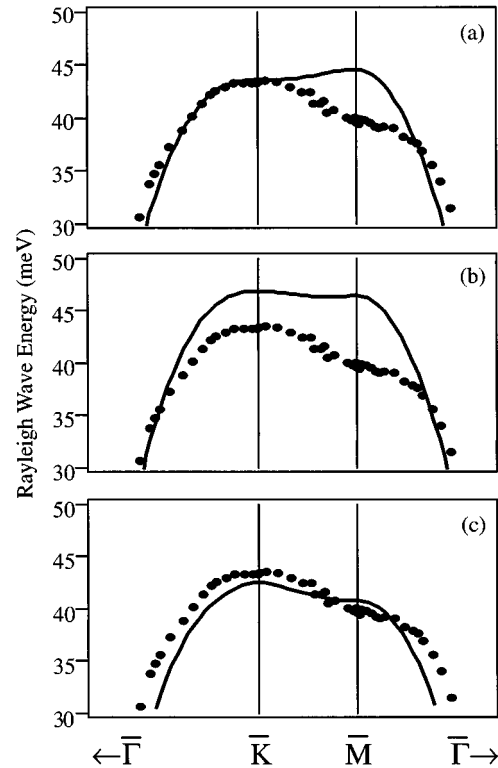


FIG. 13. Measured RW dispersion compared to that calculated using (a) the bulk-terminated model. In panel (b) the in-plane, nearest-neighbor interactions (2NN) have been replaced with a purely central interaction in the top two surface layers. In panel (c), the model is modified further by the replacement of the first-nearest-neighbor interaction (between the first two surface planes) by a central force.

sensitive to the δ_2 coupling and are unchanged. If one replaces the 1NN and 2NN interactions by purely central forces at the surface, the RW dispersion shown in panel (c) results. Specifically, the force-constant matrices for the first- and second-nearest neighbors in the top two layers of the slab have been replaced with those calculated from a simple spring model. The specific parameters chosen correspond to significantly weaker interplanar bonding, which lowers the energy of the RW throughout the zone.

One must be careful in interpreting the results of *ad hoc* force-constant modifications at the surface, especially with regards to uniqueness. In the present case, one must determine if a reversal of the sign of the RW dispersion can be brought about by varying the central parts of the interactions. As noted above, this is unlikely because the displacement patterns are similar. In Fig. 14, the energies of the surface modes at the high-symmetry points of the surface Brillouin zone are displayed as a function of the model parameters in the top layer. In panel (a), the modes are shown as a function of the central part of the interplanar interaction; that is, a “spring” has been added or subtracted from the nearest-neighbor (1NN) interaction. In panel (b), the same procedure has been applied to the 2NN in-plane interaction. In panel (c), a stretched or compressed spring has been added to the 2NN interaction. In CF models, this type of interaction is related to surface stress. Calculations²⁹ indicate that the tensile stress is very large at this surface; however, our model-

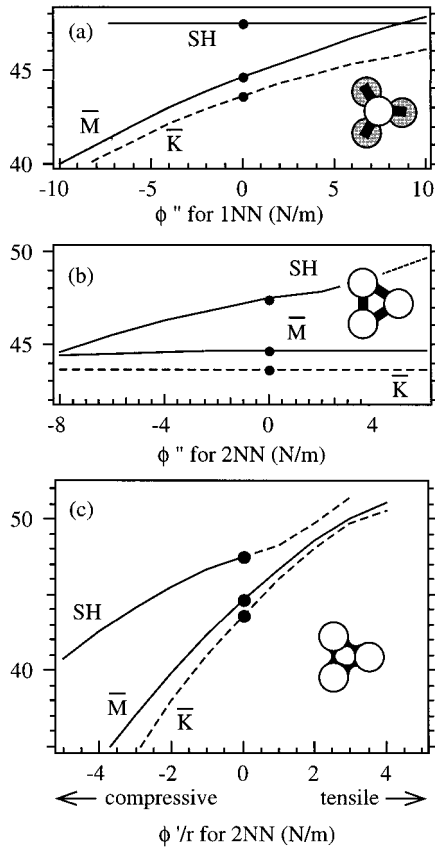


FIG. 14. Calculated surface-mode energies as a function of adding or subtracting a central force to the (a) nearest-neighbor interaction (between planes), and (b) second-nearest-neighbor interaction (in plane). Panel (c) shows the effect of adding a compressive or tensile stress term to the second-nearest-neighbor interaction.

ing indicates that surface stress alone cannot account for the sign of the dispersion from \bar{K} to \bar{M} . Stress may be the important mechanism in increasing the energy of the band of parallel modes.

As the data presented in Fig. 14 illustrate, modifying only the near-neighbor central interactions in the surface layer cannot reproduce the observed RW dispersion; that is, the ordering of the RW energies at \bar{K} and \bar{M} is not reversed. However, the average energy of the RW is a strong function of these parameters: stronger interplanar bonding increases the energy of the RW, stronger in-plane bonding increases the energy of the shear mode, as one might expect. Surface stress has a large effect on all of the modes. From these modifications we conclude that the discrepancy between the calculated BT dispersion and the measurements can only be reconciled if noncentral forces are modified at the surface. Further modifications are required in order to bring the model into quantitative agreement with the measured dispersion. Modifying the central interactions, as is shown in Fig. 14, provides one way of accomplishing this. It should be stressed, however, that the modifications required in order to bring all modes into agreement with the measured values most likely require changes to the model parameters in several layers. If, in order to reproduce the observed RW and SH dispersion, one introduces purely central interactions in only the first two layers, surface modes appear that are localized in the second and third layers, i.e., at the interface between

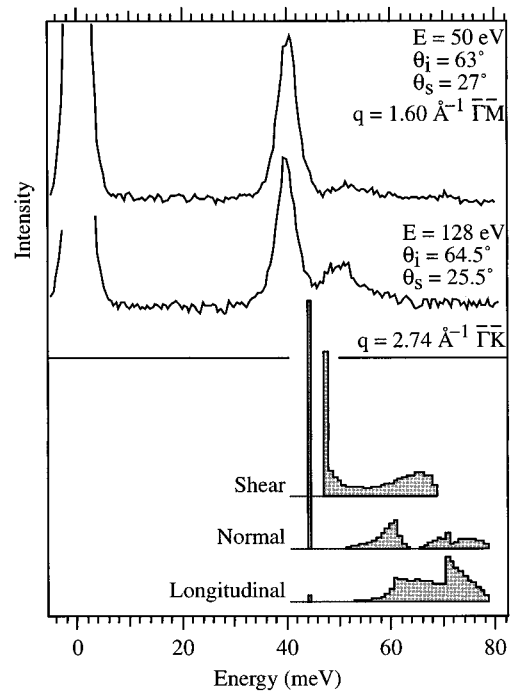


FIG. 15. EELS spectra sampling \bar{M} from two different scattering geometries. The lower panel shows the surface-weighted DOS from the bulk-terminated calculation.

the bulklike and modified layers. A more physically reasonable approach is to gradually increase the central parts of the interactions as the surface is approached from the bulk. The RW dispersion at long wavelength, as well as the core-level studies,²⁸ reinforce this view. It would be interesting to determine if these effects are predicted within a first-principles density-functional theory near the surface.

C. The shear-horizontal mode at \bar{M}

The BT calculation exhibits a band of shear-horizontal modes just at the band edge at \bar{M} , whereas the EELS data show a weak feature at \bar{M} near 50 meV, well above the bulk band edge. The geometry of the (0001) surface is such that modes at \bar{M} can be excited in two different scattering geometries (see inset to Fig. 8). The $\bar{\Gamma}-\bar{M}$ direction coincides with a mirror plane of the surface, and modes which are odd with respect to reflection in the scattering plane will not be excited using this scattering geometry. However, modes that are odd in the $\bar{\Gamma}-\bar{M}$ scattering plane have longitudinal components with respect to the $\bar{\Gamma}-\bar{K}$ direction, and can be excited. In Fig. 15, EELS spectra from \bar{M} , obtained in the two different scattering geometries, are shown superimposed on the surface-weighted DOS. The RW, with displacements almost entirely normal to the surface, is present in both spectra. However, the mode at 50 meV is more intense in the spectra obtained in the $\bar{\Gamma}-\bar{K}-\bar{M}$ geometry ($q = 2.75 \text{ \AA}^{-1}$). In the $\bar{\Gamma}-\bar{M}$ direction, a weak feature is visible at, perhaps, slightly higher energy (52 meV). From the surface-weighted DOS, shown in the lower part of the figure, it is evident that the 50 meV feature does not arise from a high density of bulk modes. In fact, below 51 meV, the entire bulk DOS at \bar{M} is due to shear modes. The weak feature at 52

meV in the *upper* spectrum may be due to the excitation of longitudinal or normal bulk modes at the band edge with unexpectedly large cross sections. However, in the $\bar{\Gamma}-\bar{K}$ direction, the “longitudinal” modes will not be excited, because they have shear character with respect to this scattering geometry. We conclude that the feature observed at 50 meV in the *lower* spectrum is due primarily to the shear-horizontal surface mode. In this scattering geometry, the shear mode is not forbidden—it has the character of a longitudinal vibration and possesses a large surface weight. Our assignment is supported by the calculated DOS, which shows that the density of perpendicular modes (i.e., those modes which could contribute in both scattering geometries) is vanishingly small, and which does show a very large feature arising from the shear-horizontal mode.

V. CONCLUSIONS

In summary, we find that the vibrational modes at the Be(0001) surface are qualitatively different from those calculated using a model that is highly successful in reproducing the bulk phonon dispersion: a Born–von Karman model that includes generalized tensor-force interactions between atoms. The experiment and theory can only be reconciled easily if noncentral forces are reduced in magnitude at the surface. We conclude that the large density of surface states is the determining factor in the electronic, structural, and dynamical properties of this surface. Given this hypothesis, that the surface states on Be(0001) are crucial to an understanding of the properties of this surface, many other experi-

mental observations can be explained. The anomalous outward expansion of this surface¹⁷ is a consequence of the fact that the isotropic surface state charge distribution allows the surface to relax back towards the ideal c/a ratio. The large, negative core level shifts at the Be(0001) surface,²⁸ compared to other metals and to the more-open Be(10 $\bar{1}$ 0) surface³³, are a result of the increased final-state screening by the surface states. Finally, the high energy of the free-electron-like multipole plasmon mode observed at the Be(0001) surface³⁴ is a direct consequence of the high density of delocalized (in the plane) surface states. Finally, we note that our conclusions concerning the importance of surface states at the Be(0001) surface can be tested by comparing the dynamics of the Be(0001) surface with those of Mg(0001) and Be(10 $\bar{1}$ 0).

ACKNOWLEDGMENTS

The development of the noncentral force model benefited significantly from discussions with M.E. Mostoller. Primary support for this work was provided by the U.S. National Science Foundation under Contract No. DMR-93-96059 (J.B.H. and E.W.P.) and by the U.S. Department of Energy under Contract No. 91-ER-45118 (E.J.M.). The experiments and calculations were performed at the Oak Ridge National Laboratory, which is funded by the Division of Material Sciences, U.S. Department of Energy, under Contract No. DE-AC05-84OR21400 with Martin Marietta Energy Systems, Inc.

*Present address: IGW, Forschungszentrum Jülich GmbH, D-52425 Jülich, Germany.

¹V. E. Bondybey and J. H. English, *J. Chem. Phys.* **80**, 568 (1984).

²W. J. Balfour and A. E. Douglas, *Can. J. Phys.* **48**, 901 (1970).

³M. Y. Chou and M. L. Cohen, *Solid State Commun.* **57**, 785 (1986).

⁴M. Y. Chou, Pui K. Lam, and M. L. Cohen, *Phys. Rev. B* **28**, 4179 (1983).

⁵T. L. Loucks and P. H. Cutler, *Phys. Rev.* **133**, A819 (1964).

⁶P. N. Keating, *Phys. Rev.* **145**, 637 (1966).

⁷W. Weber, *Phys. Rev. B* **15**, 4789 (1977).

⁸J. C. Phillips, *Phys. Rev.* **166**, 832 (1968).

⁹R. M. Martin, *Phys. Rev.* **186**, 871 (1969).

¹⁰C. S. Jayanthi, H. Bilz, and W. Kress, *Phys. Rev. Lett.* **59**, 795 (1987).

¹¹A. P. Roy, B. A. Dasannacharya, C. L. Thaper, and P. K. Iyengar, *Phys. Rev. Lett.* **30**, 906 (1973).

¹²R. Pynn and G. L. Squires, *Proc. R. Soc. London Ser. A* **326**, 347 (1971).

¹³R. Stedman, Z. Amilius, R. Pauli, and O. Sundin, *J. Phys. F* **6**, 157 (1976).

¹⁴J. L. Warren, *Rev. Mod. Phys.* **40**, 38 (1968).

¹⁵E. Wimmer, *J. Phys. F* **14**, 681 (1984).

¹⁶J. C. Boettger and S. B. Trickey, *Phys. Rev. B* **32**, 1356 (1985).

¹⁷H. L. Davis, J. B. Hannon, K. B. Ray, and E. W. Plummer, *Phys. Rev. Lett.* **68**, 2632 (1992).

¹⁸M. W. Finnis and V. Heine, *J. Phys. F* **4**, L37 (1974).

¹⁹A. G. Eguluz, A. A. Maradudin, and R. F. Wallis, *Phys. Rev. Lett.* **60**, 309 (1988).

²⁰J. A. Gaspar and A. G. Eguluz, *Phys. Rev. B* **40**, 11 976 (1989).

²¹E. V. Chulkov, V. M. Silkin, and E. N. Shirykalov, *Surf. Sci.* **188**, 287 (1987).

²²A. A. Maradudin and S. H. Vosko, *Rev. Mod. Phys.* **40**, 1 (1968).

²³A. A. Maradudin, E. W. Montroll, G. H. Weiss, and I. P. Ipatova, in *Solid State Physics: Advances in Research and Applications*, edited by H. Ehrenreich, F. Seitz, and D. Turnbull (Academic Press, New York, 1971), Suppl. 3.

²⁴M. E. Mostoller has suggested that this is related to the fact that fourth-nearest-neighbor interaction links neighboring “A” planes in the *A-B-A-B* hcp stacking sequence, and is important in differentiating the hcp and fcc crystal structures.

²⁵R. L. Sameth, Master’s thesis, University of Pennsylvania, 1992.

²⁶J. B. Hannon and E. W. Plummer, *J. Electron. Spectrosc. Relat. Phenom.* **64/65**, 683 (1993).

²⁷The longitudinal mode is not a surface mode according to the strict definition given in the text. The surface weight is less than 15%.

²⁸L. I. Johansson, H. I. P. Johansson, J. N. Andersen, E. Lundgren, and R. Nyholm, *Phys. Rev. Lett.* **71**, 2453 (1993).

²⁹R. Stumpf, J. B. Hannon, P. J. Feibelman, and E. W. Plummer, in *Proceedings of the 134th Heraeus Seminar* (World Scientific, Philadelphia, 1995).

³⁰R. Nyholm, J. N. Andersen, J. F. van Acker, and M. Quarford, *Phys. Rev. B* **41**, 10 987 (1991).

³¹R. J. Needs and M. J. Godfrey, Phys. Scr. **T19**, 391 (1987).

³²A catalog of measured surface-phonon dispersion can be found in *Surface Phonons*, edited by W. Kress and F. W. deWette, Springer Series in Surface Science Vol. 21 (Springer, Berlin, 1991).

³³H. I. P. Johansson, L. I. Johansson, E. Lundgren, J. N. Andersen, and R. Nyholm, Phys. Rev. B **49**, 17 460 (1994).

³⁴R. A. Bartynski, E. Jensen, T. Gustafsson, and E. W. Plummer, Phys. Rev. B **32**, 1921 (1985).